LES with wall models for trailing-edge aeroacoustics

By Meng Wang

1. Motivation and objectives

This work deals with the numerical simulation of turbulent boundary layer flows past a 25-degree, asymmetric trailing edge of a model airfoil, investigated experimentally by Blake (1975). The Reynolds number based on free-stream velocity U_∞ and the airfoil chord C is 2.15×10^6. The objective is to develop effective numerical prediction methods, based on a combination of large-eddy simulation (LES) and Lighthill's acoustic analogy, for trailing-edge noise and surface pressure fluctuations.

A major difficulty encountered in previous studies (Wang 1998, Wang & Moin 1999) is the high computational cost of the source-field simulation given the relatively high Reynolds number and complex geometry. More than 200 single processor CPU hours were needed on CRAY C-90 to advance the simulation by one flow-through time even though the computational domain contained only the rear 38% of the model airfoil chord and the near wake of approximately equal length. The spanwise domain width is only 50% of the airfoil thickness, which is too restrictive to allow the development of fully three-dimensional flow structures in the separated region near the trailing edge. As a result, while this computational domain is adequate for predicting noise in the intermediate to high frequency ranges, the spanwise source coherence does not decay sufficiently at low frequencies, suggesting the need for a wider computational domain.

In order to allow for domain expansion and to be able to compute even higher Reynolds number flows of interest in naval applications, significant speedup of the source-field simulation is needed. To this end, a new approach in which the LES is conducted in conjunction with wall-layer models has been explored. The use of wall models reduces computational cost by removing the near-wall resolution requirement. The LES is conducted on a relatively coarse grid with the first off-wall grid point typically located in the logarithmic region. The effect of the unresolved near-wall layer (viscous and buffer regions) is determined from a wall model calculation, which provides the approximate boundary conditions in the form of instantaneous wall shear-stresses for the outer flow LES. The development of wall models for LES has been an active area of research in recent years, and a number of wall models have been proposed by CTR researchers (e.g., Cabot 1995, 1996, 1997; Cabot & Moin 1999; Nicoud *et al.* 1999). The trailing-edge flow provides a challenging case to test the performance of these models in the presence of strong pressure gradient and unsteady separation. In the present work, a simple equilibrium stress balance model coupled with a mixing-length eddy viscosity, with or without pressure gradient imposed from the outer LES solution, is employed. The predicative capabilities of this hybrid LES/wall-modeling approach for flow separation, surface pressure fluctuations, and radiated noise are evaluated.

2. Accomplishments

2.1 Simulation method

The basic numerical method and simulation procedure are described in Wang (1998) and hence not repeated here. In the new simulations with wall models, the same computational domain of $16.5h \times 41h \times 0.5h$, where h denotes the airfoil thickness, is used, while the grid is reduced to $768 \times 64 \times 24$, 1/6 of the original size. Specifically, the grid is coarsened by 1/2 in both the streamwise (x_1) and spanwise (x_3) directions and by 1/3 in the wall-normal (x_2) direction. The first off-wall velocity nodes (on staggered mesh) are located at, in wall units, $x_2^+ \approx 60$ for u_2 and $x_2^+ \approx 30$ for u_1 and u_3 near the computational inlet. The latter position corresponds to the lower edge of the logarithmic layer. Note that the new grid size is chosen to resolve the desired flow scales in the outer layer and is thus not strongly dependent on the Reynolds number. The same grid size can be expected applicable to higher Reynolds number flows.

The mean inflow velocity profiles used for the previous LES are interpolated onto the coarser grid for the present simulations. The time-dependent inflow data in the boundary layers on the upper and lower surfaces are interpolated in both space and time and fed into the new simulations with larger time steps. The total reduction in CPU time by the use of wall-models, due both to the smaller grid size and larger time steps, is over 90% compared to the full LES.

Since the simulation does not resolve the viscous sublayer, approximate wall boundary conditions are needed. The velocity component u_2 normal to the wall is set to zero. In the directions tangential to the wall, instead of imposing the no-slip condition, the wall shear stress components τ_{w1} and τ_{w3}, determined from a suitable wall model, are imposed.

Following Cabot (1995) and Balaras, Benocci, & Piomelli (1996), the equations governing the wall-layer flow is approximated by the boundary layer equations,

$$\frac{\partial}{\partial x_2}\left(\nu + \nu_t\right)\frac{\partial u_i}{\partial x_2} = F_i, \qquad i = 1, 3 \tag{1}$$

where in general

$$F_i = \frac{1}{\rho}\frac{\partial p}{\partial x_i} + \frac{\partial u_i}{\partial t} + \frac{\partial}{\partial x_j}u_i u_j. \tag{2}$$

The pressure is assumed x_2-independent, equal to the value from the outer-flow LES solution. The eddy viscosity ν_t in the wall layer is obtained from a Reynolds-Averaged Navier Stokes (RANS) type model (Cabot 1995): $\nu_t = \kappa u_\tau y_w D^2$; $D = 1 - \exp(-u_\tau y_w / A\nu)$, where κ, u_τ, and y_w are the von Karman constant, friction velocity, and distance to the wall, respectively, and $A = 17$. Equation (1) is required to satisfy

$$x_2 = 0, \quad u_i = 0; \qquad x_2 = \delta, \quad u_i = u_{\delta i}. \tag{3}$$

where $u_{\delta i}$ denotes the outer flow velocity from LES at the first off-wall velocity node $x_2 = \delta$.

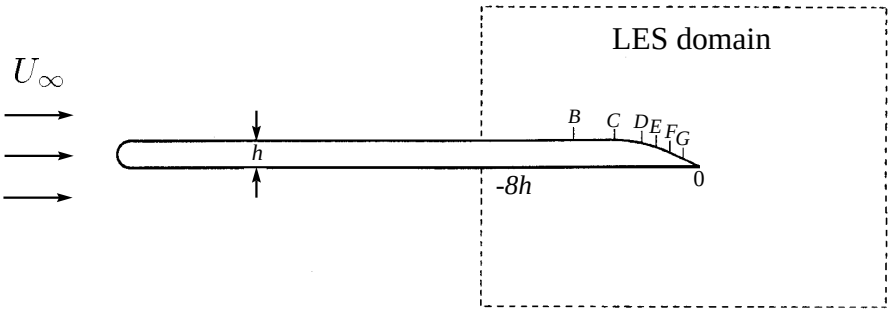

FIGURE 1. Trailing-edge geometry and measurement stations. Stations B–G are located at $x_1/h = -4.625$, -3.125, -2.125, -1.625, -1.125, and -0.625, respectively.

The partial differential equation system (1)-(3) in general needs to be solved numerically along with the outer flow LES. However, if the substantial derivative term in F_i is ignored, (1) can be integrated analytically to give

$$\tau_{wi} = \mu \frac{\partial u_i}{\partial x_2}\bigg|_{x_2=0} = \frac{\rho}{\int_0^\delta \frac{dx_2}{\nu+\nu_t}} \left\{ u_{\delta_i} - F_i \int_0^\delta \frac{x_2}{\nu+\nu_t} dx_2 \right\}. \tag{4}$$

In particular, if $F_i = 0$, the model implies the logarithmic law of the wall for the instantaneous velocities for $\delta^+ \gg 1$ and linear velocity distributions for $\delta^+ \ll 1$.

In the present study, we evaluate the performance of the above wall model when progressively better approximations are made about F_i. The results presented below are for the cases $F_i = 0$ and $F_i = \frac{1}{\rho}\frac{\partial p}{\partial x_i}$. Simulations using the full boundary layer equations (all terms in (2)) are under way, and will be reported in the future.

2.2 Results and discussion

The trailing-edge geometry and measurement stations in Blake's experiment are depicted in Fig. 1. The positions B, C, D, E, F, and G are located at $x_1/h = -4.625$, -3.125, -2.125, -1.625, -1.125, and -0.625, respectively, in a Cartesian coordinate system originating from the trailing edge.

In Fig. 2 the mean velocity magnitude computed using wall models with $F_i = 0$ (solid lines) and $F_i = \frac{1}{\rho}\frac{\partial p}{\partial x_i}$ (dashed lines) are compared with those from the full LES (dotted lines) and Blake's experiment (symbols) at measurement stations C–G and the trailing edge. The velocity magnitude, defined as $U = (U_1^2 + U_2^2)^{1/2}$, is normalized by its value U_e at the boundary-layer edge. The vertical coordinate is measured as the vertical distance to the upper surface. The overall agreement is good, particularly among the results from the full LES and those from LES with wall models. The two different wall models used give nearly identical results upstream of station E, where the turbulent boundary layer remains attached. They are also seen to predict the separation near the trailing-edge reasonably well. Downstream of the separation point (station F), the model which incorporates the pressure gradient term shows improved results relative to the one without pressure gradient.

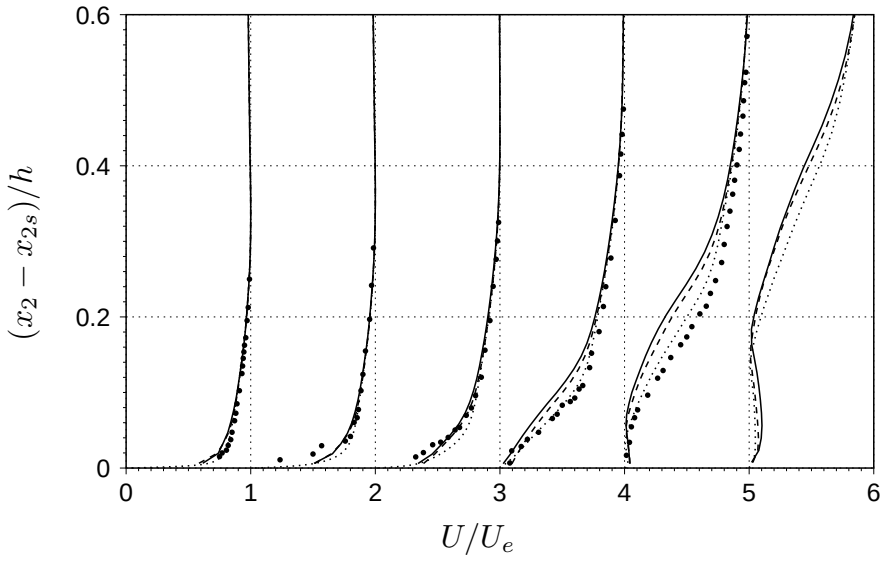

FIGURE 2. Profiles of the normalized mean velocity magnitude as a function of vertical distance from the upper surface, at stations (from left to right) C, D, E, F, G, and trailing-edge. ——— LES with wall model ($F_i = 0$); - - - - LES with wall model ($F_i = \frac{1}{\rho}\frac{\partial p}{\partial x_i}$); ····· full LES; • Blake's experiment. Individual profiles are separated by a horizontal offset of 1 with the corresponding zero lines located at 0, 1, ..., 5.

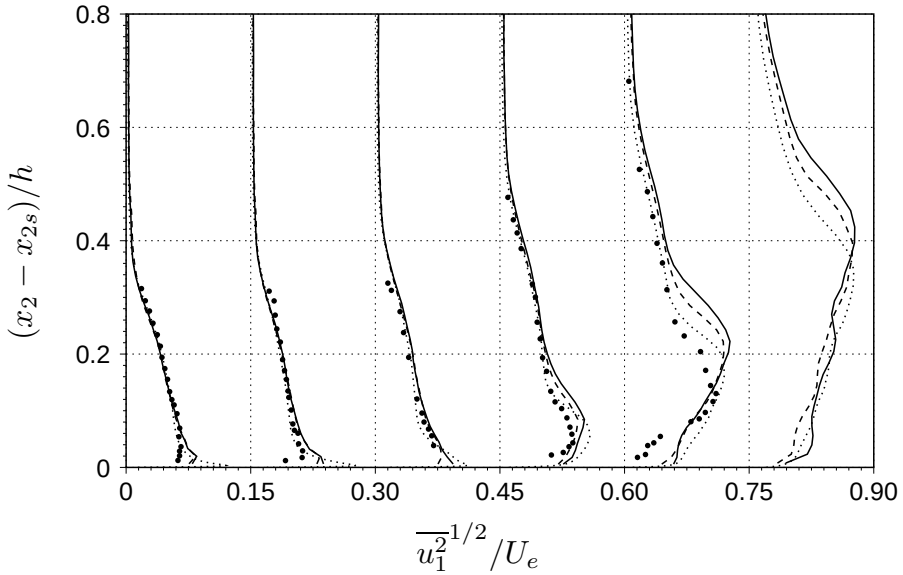

FIGURE 3. Profiles of the rms streamwise velocity fluctuations as a function of vertical distance from the upper surface, at stations (from left to right) B, D, E, F, G, and trailing-edge. ——— LES with wall model ($F_i = 0$); - - - - LES with wall model ($F_i = \frac{1}{\rho}\frac{\partial p}{\partial x_i}$); ····· full LES; • Blake's experiment. Individual profiles are separated by a horizontal offset of 0.15 with the corresponding zero lines located at 0, 0.15, ..., 0.75.

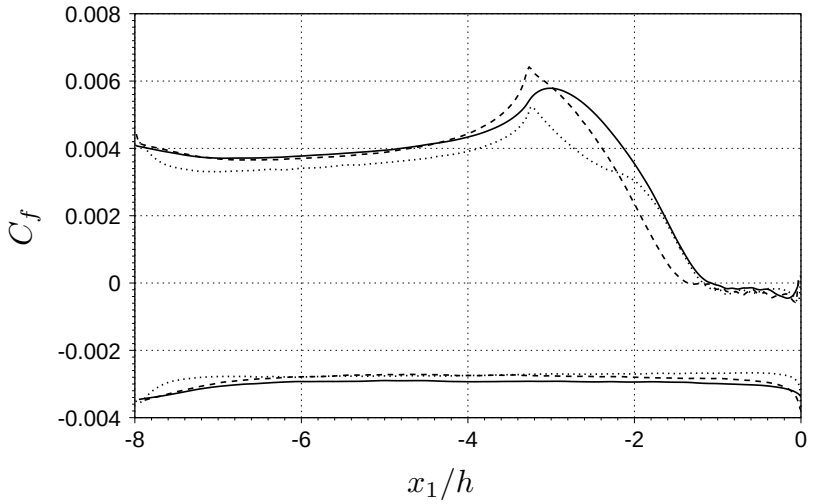

FIGURE 4. Distribution of the mean skin friction coefficient near the trailing edge. ——— LES with wall model ($F_i = 0$); – – – – LES with wall model ($F_i = \frac{1}{\rho}\frac{\partial p}{\partial x_i}$); ····· full LES.

The profiles of the rms streamwise velocity fluctuations normalized by U_e, at stations (from left to right) B, D, E, F, G, and the trailing-edge, are plotted in Fig. 3. As in the case of mean velocities, the wall model with imposed pressure gradient (dashed lines) gives more accurate rms fluctuations in the separated region than that without pressure gradient (solid lines). However, significant discrepancies with the full LES predictions (dotted lines) and the experimental data (symbols) still exist. The intensity peak and its distance to the wall are overpredicted (e.g. station G), which has implications to the wall-pressure spectral characteristics as will be shown later. In the attached boundary layer (station E and those upstream of it), the two wall-model based LES solutions are nearly the same. Both agree well with the full LES and experimental data except that they are unable to resolve the intensity peak which lies below the first off-wall grid point.

The skin friction coefficient $C_f = 2\tau_w/\rho U_\infty^2$ is shown in Fig. 4. On the lower surface (lower curves) as well as the flat section of the upper surface (upper curves), the wall model predictions track closely the C_f curves computed from the full LES (experimental data are unavailable). The values are shifted, however, by up to 10% on the upper flat surface. This appears to be caused by the different transient responses to the time dependent inflow condition. As the upper boundary-layer flow enters the region with strong favorable pressure gradient (cf. Fig. 5), the wall model with pressure gradient predicts the correct qualitative behavior of C_f, including the peak and its location. Significant deviations occur downstream of the C_f peak where the flow undergoes a favorable-to-adverse pressure gradient transition. Further downstream, however, the C_f curve from the wall model without pressure gradient shows excellent agreement with that from the full LES while significant error remains in the the prediction by the model with pressure gradient. The agreement is likely caused by a fortuitous cancellation between the pressure gradient term and the convective terms which are not included in the calculations.

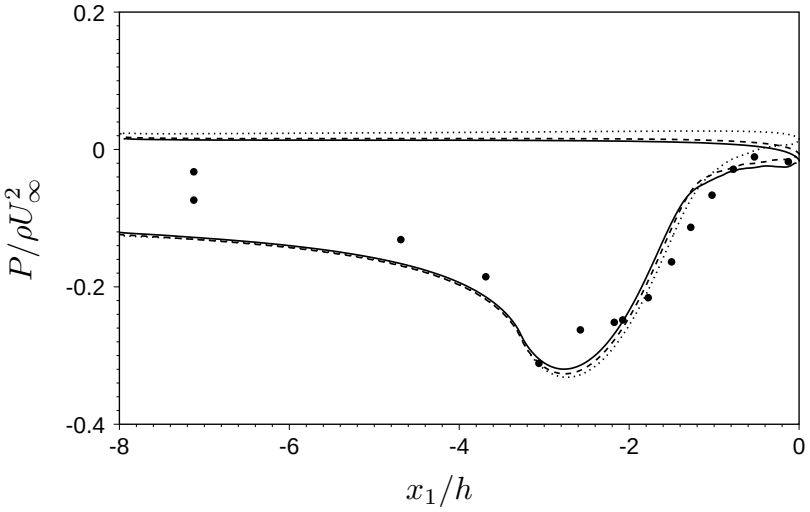

FIGURE 5. Mean surface pressure distribution near the trailing edge. ——— LES with wall model ($F_i = 0$); - - - - LES with wall model ($F_i = \frac{1}{\rho}\frac{\partial p}{\partial x_i}$); ····· full LES; • Blake's experiment.

Figure 4 illustrates again that the wall model approach predicts the separated region (negative C_f) well because the near-wall layer is much thicker in this region and is hence resolved despite the coarse grid.

The mean pressure distributions along the trailing-edge surface are plotted in Fig. 5. The differences among solutions from the full LES (dotted line) and from LES in conjunction with wall models (solid and dashed lines) are rather small because the mean surface pressure is predominantly determined by the potential flow outside the boundary layers (although the trailing-edge separation and wake structure also play a role). The large discrepancy between the computational and experimental values, particularly near the inflow boundary, is a result of the different inflow velocity conditions (Wang 1998).

Figure 6 depicts the frequency spectra of surface pressure fluctuations obtained from LES in conjunction with the wall model with pressure gradient and compares them with those from the full LES and Blake's experiment. The variable q_∞ used in the normalization is the dynamic pressure, defined as $\rho U_\infty^2/2$. Except for the narrower resolvable frequency ranges due to the coarser grid, the accuracy of the new predictions are comparable with those from the full LES in the favorable pressure gradient region (station *C*), adverse pressure gradient region (station *E*), and separation point (station *F*). Inside the separated region (station *G*), the pressure spectra are significantly overpredicted at low frequencies by the full LES and even more so by the LES with wall model. This is believed to be related primarily to the inaccurate fluctuating velocity profiles shown in Fig. 3. An overprediction of the rms velocity fluctuations at large distances to the wall causes the exaggeration of large-scale flow structures, which are responsible for the low frequency portion of the wall pressure spectrum. Other sources of error may arise from the approximation of wall pressure by the cell-centered values adjacent to the wall and from

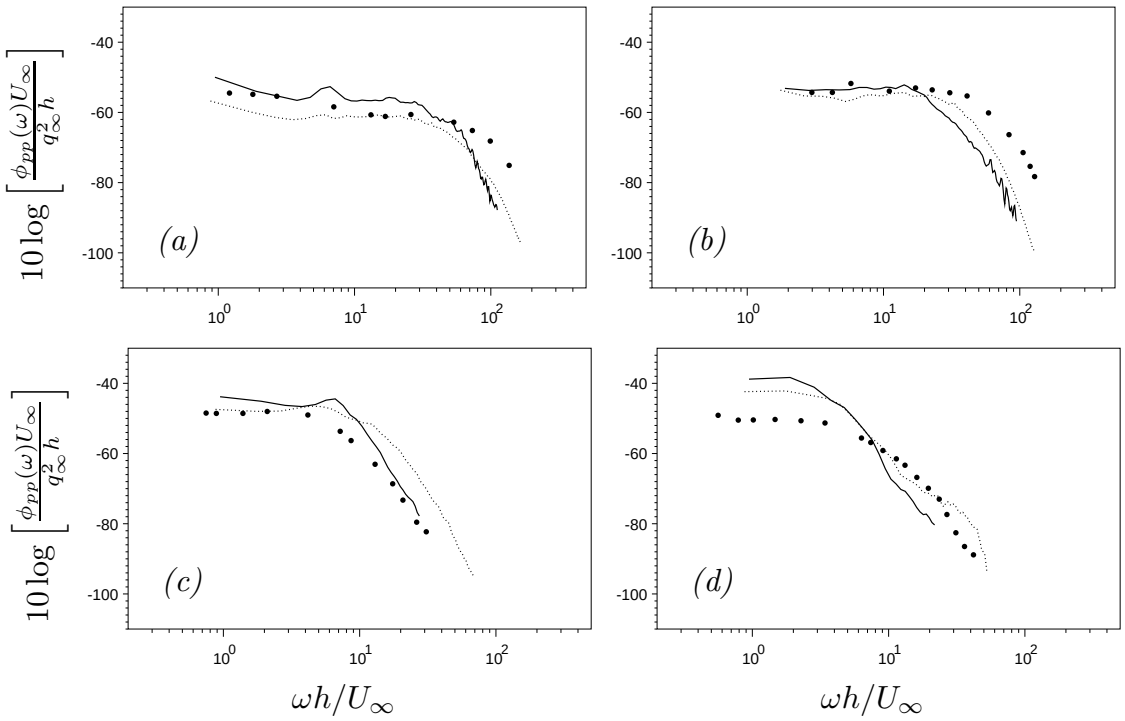

FIGURE 6. Frequency spectra of wall pressure fluctuations at stations (a) C; (b) E; (c) F; and (d) G. ——— LES with wall model ($F_i = \frac{1}{\rho}\frac{\partial p}{\partial x_i}$); ····· full LES; • Blake's experiment.

the fact that, in the present LES formulation, the "pressure" actually contains the subgrid-scale kinetic energy. The latter is negligibly small in the first off-wall pressure node if the wall layer is resolved but may not be negligible in the present case because of the coarse mesh. This effect needs to be further investigated.

The source-field data obtained from LES with the wall model with pressure gradient are used to compute the acoustic far-field, based on Lighthill's theory (Lighthill 1952) and an approximate Green's function for a rigid, semi-infinite, thin plate (Ffowcs Williams & Hall 1970). The evaluation method is basically the same as in Wang (1998) except that the spanwise compactness of the source region is exploited to simplify the calculations. The acoustic pressure in the far-field can be approximated by, in the frequency domain,

$$\widehat{p}_a(\mathbf{x},\omega) \approx \frac{e^{i\left(k|\mathbf{x}|-\frac{\pi}{4}\right)}}{2^{\frac{5}{2}}\pi^{\frac{3}{2}}\,|\mathbf{x}|}\,(k\sin\phi)^{\frac{1}{2}}\sin\frac{\theta}{2}\;\widehat{S}(\omega); \tag{5}$$

$$S(t) = \int_V \frac{\rho_\infty}{r_0^{\frac{3}{2}}}\left\{\left(u_\theta^2 - u_r^2\right)\sin\frac{\theta_0}{2} - 2u_r u_\theta\cos\frac{\theta_0}{2}\right\} d^3\mathbf{y}, \tag{6}$$

where $\mathbf{x}$ (r, θ, z) and $\mathbf{y}$ (r_0, θ_0, z_0) represent far-field and source-field positions, respectively. The velocity components u_r and u_θ are defined in a cylindrical-polar coordinate system where the z coordinate coincides with the trailing-edge and θ

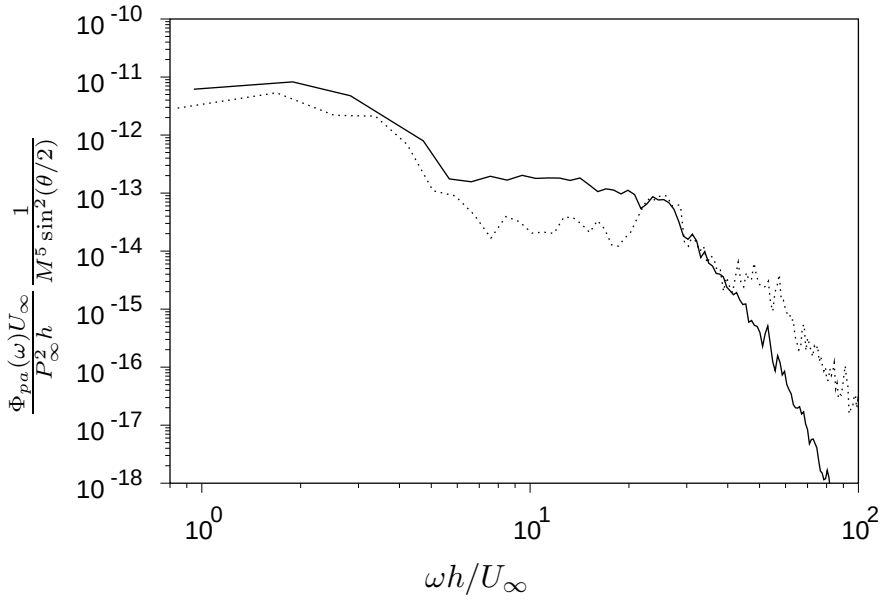

FIGURE 7. Frequency spectra of the far-field noise at $r/h = 150$ and $M = 0.088$ from sources within the LES domain. ——— source field computed using LES with wall model ($F_i = \frac{1}{\rho}\frac{\partial p}{\partial x_i}$); - - - - source field computed using full LES.

is measured counter-clockwise from the downstream direction. The caret denotes temporal Fourier transform, ω is the circular frequency, $k = \omega/c_\infty$ is the acoustic wavenumber, and $\sin\phi = r/|\mathbf{x}|$. Equation (5) is particularly convenient to use because, rather than dealing with spatially distributed source terms, it involves only a single compact source $S(t)$ which can be easily evaluated during the source field LES.

The noise spectrum obtained using LES with wall model ($F_i = \frac{1}{\rho}\frac{\partial p}{\partial x_i}$) is shown in Fig. 7 as the solid line along with that from the earlier full LES calculation (dotted line). The spectra are calculated for $r/h = 150$ and $M = 0.088$ and account for contributions from the source region within the computational domain only. The two spectral curves show reasonable agreement at low frequencies. However, significant discrepancy exists for $6 \leq \omega h/U_\infty \leq 20$, a frequency range likely dominated by the large scale eddies from the unsteady separation on the upper side of the edge. For $\omega h/U_\infty \geq 20$, the spectra are dominated by the diffraction of boundary-layer eddies from the lower side. The two calculations agree well until the effect of the different grid resolution becomes apparent.

It should be pointed out that Fig. 7 is used to examine the effect of source-field wall modeling on the computed far-field noise. This effect should not be altered fundamentally by the approximate Green's function. The half-plane Green's function implies that the acoustic wavelength is much longer than the thickness of the airfoil but much shorter than the chord ($h \ll \lambda_a \ll C$), which corresponds to $3 \ll \omega h/U_\infty \ll 70$, approximately. The effect of finite chord, which is particularly severe at low frequencies, can be accounted for by Howe's (1999a) multiple scattering analysis. Furthermore, even though the airfoil is acoustically thin, the neglect

of the detailed trailing edge shape relative to the source distribution introduces an additional source of error, which can be significant at high frequencies (Howe 1999b, 1999c). If more accurate solutions are desired, a shape-dependent Green's function should be employed, which can be obtained computationally following the analysis of Howe (1999b).

3. Summary and future work

As discussed in Wang (1998), the two major impediments to accurate predictions of the trailing-edge flow and noise are: (1) the high computational cost, which has severely limited the computational domain size in the streamwise and spanwise directions; (2) the uncertainty about the velocity profiles at the computational inflow boundary, which are not available from Blake's experiment.

To speed up the near-field LES, two steps have been taken. First, the serial code, originally written for CRAY, has been ported to a multiprocessor SGI Origin 2000 platform, optimized, and parallelized using OpenMP. This results in much faster turnaround time and allows us to perform larger simulations. Secondly, the use of wall models in conjunction with LES for the source-field computation has been explored.

LES with wall-modeling offers a cost effective means of computing high Reynolds number flows encountered in naval applications. The results presented in this report are encouraging. A simple stress balance model coupled with a mixing-length eddy viscosity, with or without pressure gradient imposed from the outer LES solution, is found to predict velocity statistics fairly well compared with those from the full LES, at less than 10% of the original computational cost. In particular, the separation point near the trailing-edge is predicted correctly. The surface-pressure and noise spectra predictions appear promising. However, large discrepancies with the full LES solutions remain in the separated region and within certain frequency ranges. We will continue to pursue the wall-modeling approach with more elaborate models, including that based on the full boundary layer equations (1) and (2). A critical assessment of the suitability and accuracy of this approach for calculating the unsteady wall-pressure and noise will be conducted.

To address the issue of inflow conditions, a new experiment has been commissioned by ONR at the University of Notre Dame (Blake & Mueller 1999, private communication), which will provide accurate measurements of the velocity profiles at the inlet of the computational domain. We will work closely with the experimentalists and perform simulations with new boundary conditions in a wider computational domain.

REFERENCES

Balaras, E., Benocci, C., & Piomelli, U. 1996 Two-layer approximate boundary conditions for large-eddy simulation. *AIAA J.* **34,** 1111-1119.

Blake, W. K. 1975 A statistical description of pressure and velocity fields at the trailing edge of a flat strut, *DTNSRDC Report 4241,* David Taylor Naval Ship R & D Center, Bethesda, Maryland.

Cabot, W. 1995 Large-eddy simulations with wall-models. *Annual Research Briefs-1995,* Center for Turbulence Research, NASA/Stanford Univ., 41-50.

Cabot, W. 1996 Near-wall models in large-eddy simulations of flow behind a backward-facing step. *Annual Research Briefs–1996,* Center for Turbulence Research, NASA/Stanford Univ., 199-210.

Cabot, W. 1997 Wall models in large-eddy simulation of separated flow. *Annual Research Briefs–1997,* Center for Turbulence Research, NASA/Stanford Univ., 97-106.

Cabot, W. & Moin, P. 1999 Approximate wall boundary conditions in the large-eddy simulation of high Reynolds number flow. Submitted to *J. Flow, Turbulence and Combustion.*

Ffowcs Williams, J. E. & Hall, L. H. 1970 Aerodynamic sound generation by turbulent flow in the vicinity of a scattering half plane. *J. Fluid Mech.* **40,** 657-670.

Howe, M. S. 1999a Edge-source acoustic Green's function for an airfoil of arbitrary chord, with application to trailing-edge noise, *Report AM-99-010,* College of Engineering, Boston University.

Howe, M. S. 1999b Trailing-edge noise at low Mach numbers. *J. Sound Vib.* **225,** 211-238.

Howe, M. S. 1999c Trailing-edge noise at low Mach numbers, part 2: attached and separated edge flows. Submitted to *J. Sound Vib.*

Lighthill, M. J. 1952 On sound generated aerodynamically; I. General theory. *Proc. R. Soc. Lond.* A. **211,** 564-587.

Nicoud, F., Baggett, J., Moin, P., & Cabot, W. 1999 LES wall-modeling based on optimal control theory. Submitted to *Phys. Fluids.*

Wang, M. 1998 Computation of trailing-edge noise at low Mach number using LES and acoustic analogy. *Annual Research Briefs–1998,* Center for Turbulence Research, NASA/Stanford Univ., 91-106.

Wang, M. & Moin, P. 1999 Computation of trailing-edge noise using large-eddy simulation. Submitted to *AIAA J.*